

QUINTESSENCE: QUADRATIC POTENTIALS

ARTUR ALHO,^{1*} CLAES UGGLA^{2†}

¹*Center for Mathematical Analysis, Geometry and Dynamical Systems,*

Instituto Superior Técnico, Universidade de Lisboa,

Av. Rovisco Pais, 1049-001 Lisboa, Portugal.

²*Department of Physics, Karlstad University,*

S-65188 Karlstad, Sweden.

November 15, 2025

Abstract

Arguably one can use a canonical scalar field φ , minimally coupled to gravity, with quadratic potentials $V = \Lambda \pm \frac{1}{2}m^2\varphi^2$ to explore some general features of slow-roll and hilltop thawing quintessence, respectively. For each of these two potentials, and pressure-free matter, we introduce a regular unconstrained dynamical system on a compact state space, where the formulation for the hilltop case is new. Together with a derivation of monotonic functions in the two global state space settings, this enables us to obtain global results and to introduce figures that illustrate the global solution spaces of these models, in which we situate the observationally viable quintessence solutions.

*Electronic address: aalho@math.ist.utl.pt

†Electronic address: claes.uggla@kau.se

1 Introduction

Over the last ~ 30 years the Λ CDM model with a dark energy (DE) equation of state parameter $w_{\text{DE}} = w_{\Lambda} = -1$ has been the standard model in cosmology. Recent observations, however, such as the Baryonic Acoustic Oscillations (BAO) by the DESI collaboration [1], suggest that w_{DE} might be evolving. A simple and theoretically appealing dynamical DE component is a canonical scalar field, φ , minimally coupled to gravity, generally referred to as quintessence. By Taylor expanding a potential and redefining the scalar field by an appropriate translation to complete the square one generically obtains $V(\varphi) \approx \Lambda \pm \frac{1}{2}m^2\varphi^2$. In, e.g., [2] and [3] it was therefore argued that such potentials describe generic observational features of quintessence. For this reason we will introduce *regular unconstrained dynamical systems on compact state spaces* to describe the global dynamics of quintessence models for which

$$V(\varphi) = \Lambda \pm \frac{1}{2}m^2\varphi^2, \quad \Lambda > 0, \quad (1)$$

where $\Lambda > 0$ is required in order to have the Λ CDM solution as a special case, see Figure 1. Note that these potentials are invariant under the transformation $\varphi \mapsto -\varphi$,

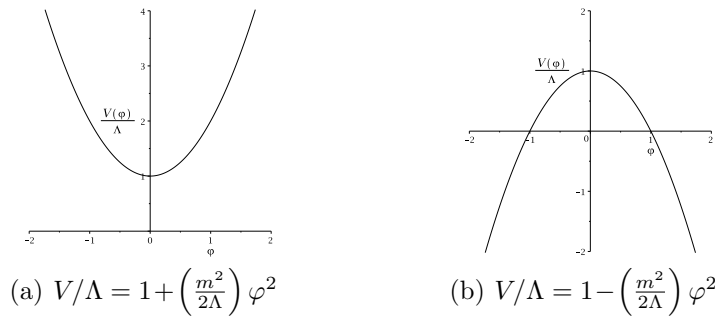


Figure 1: The potentials $V = \Lambda \pm \frac{1}{2}m^2\varphi^2$.

which results in a discrete symmetry in the dynamical systems formulations below.

We further restrict considerations to spatially homogeneous, isotropic and flat spacetimes with a source that apart from the scalar field φ also consists of matter with an energy density $\rho_m > 0$ and no pressure $p_m = 0$, representing, primarily, cold dark matter (CDM).¹ This leads to that the general relativistic Friedmann and Raychaudhuri equations; the (non-linear) Klein-Gordon equation, and energy conservation

¹This matter model is useful for describing the transition from an epoch of matter-domination to one in which the scalar field is dominant. A more realistic model involves both matter and radiation, where an epoch of radiation-domination precedes that of matter-domination. Although generalizing the discussion to include radiation is straightforward, it leads to four-dimensional state spaces instead of the present three-dimensional ones. For simplicity and pedagogically illustrative reasons we therefore neglect radiation in this paper.

for matter with $p_m = 0$, can be written as²

$$3H^2 = \rho, \quad (2a)$$

$$\dot{H} + H^2 = -\frac{1}{6}(\rho + 3p), \quad (2b)$$

$$\ddot{\varphi} = -3H\dot{\varphi} - V_{,\varphi}, \quad (2c)$$

$$\dot{\rho}_m = -3H\rho_m, \quad (2d)$$

where an overdot represents the derivative with respect to the cosmic time t ; the Hubble variable is defined by $H = \dot{a}/a$, where $a(t)$ is the cosmological scale factor, and where the total energy density ρ and pressure p are given by

$$\rho = \rho_\varphi + \rho_m, \quad p = p_\varphi, \quad (3a)$$

$$\rho_\varphi = \frac{1}{2}\dot{\varphi}^2 + V(\varphi), \quad p_\varphi = \frac{1}{2}\dot{\varphi}^2 - V(\varphi). \quad (3b)$$

Since (2a), (2b) and (3) yield

$$\dot{H} = -\frac{1}{2}(\rho + p) = -\frac{1}{2}(\rho_m + \dot{\varphi}^2) < 0, \quad (4)$$

it follows that H is monotonically decreasing. For positive scalar field potentials equation (2a) implies that H cannot change sign since $\rho > 0$ in this case and as a consequence there are two disjoint state space components: one with $H < 0$ and one forming the cosmologically relevant $H > 0$ state space. This is no longer the case when the scalar field potential can change sign from positive to negative, as for $V = \Lambda - \frac{1}{2}m^2\varphi^2$, since this implies that ρ can change sign, which results in a single connected state space.

In this paper we introduce regular dynamical systems on three-dimensional compact state spaces and use dynamical systems methods to study the global solution space properties, with a focus on quintessence ‘attractor’ solutions. The next section deals with the case $V = \Lambda + \frac{1}{2}m^2\varphi^2$ while the subsequent one addresses $V = \Lambda - \frac{1}{2}m^2\varphi^2$.

2 Models with $V = \Lambda + \frac{1}{2}m^2\varphi^2$

2.1 Dynamical systems derivation

We follow [4] and define the variables u and v according to

$$u = \frac{\varphi'}{\sqrt{3\Omega_\varphi}}, \quad v = \sqrt{\frac{\Omega_\varphi}{3}}, \quad (5)$$

where Ω_φ is the Hubble-normalized scalar field energy density, i.e.,

$$\Omega_\varphi = \frac{\rho_\varphi}{3H^2}, \quad (6)$$

²We use units such that $c = 1$ and $8\pi G = 1$, where c is the speed of light and G is the gravitational constant.

while the ' refers to the derivative w.r.t. the e -fold time

$$N = \ln(a/a_0), \quad (7)$$

where subscripts $_0$ henceforth refer to the present time $t = t_0$ and thus $a_0 = a(t_0)$ and $t = t_0 \Rightarrow N = 0$. The definition (7) implies that $N \rightarrow -\infty$ and $N \rightarrow +\infty$ when $a \rightarrow 0$ and $a \rightarrow \infty$, respectively. It follows that

$$\varphi' = 3uv, \quad \Omega_\varphi = 3v^2, \quad w_\varphi = \frac{p_\varphi}{\rho_\varphi} = u^2 - 1, \quad (8)$$

and

$$-\sqrt{2} \leq u \leq \sqrt{2}, \quad 0 \leq v \leq 1/\sqrt{3}. \quad (9)$$

Next we introduce a new bounded scalar field variable $\bar{\varphi}$ according to

$$\bar{\varphi} = 2 \arctan(\bar{m} \varphi), \quad \varphi = \bar{m}^{-1} \tan\left(\frac{\bar{\varphi}}{2}\right), \quad (10)$$

where $\bar{\varphi} \in [-\pi, \pi]$ and \bar{m} is defined as

$$\bar{m} = \frac{m}{\sqrt{2\Lambda}}. \quad (11)$$

The definitions (5), (10) and the equations in (2) or, alternatively, the general equations in [4] for bounded

$$\lambda = -\frac{V_{,\varphi}}{V}, \quad (12)$$

where in the present case

$$\lambda = -\bar{m} \sin \bar{\varphi}, \quad \frac{d\bar{\varphi}}{d\varphi} = \bar{m}(1 + \cos \bar{\varphi}), \quad (13)$$

lead to the following three-dimensional unconstrained *regular* dynamical system for $(\bar{\varphi}, u, v)$:

$$\bar{\varphi}' = 3\bar{m}(1 + \cos \bar{\varphi})uv, \quad (14a)$$

$$u' = -\frac{3}{2}(2 - u^2)(u + \bar{m}v \sin \bar{\varphi}), \quad (14b)$$

$$v' = \frac{3}{2}(1 - u^2)(1 - 3v^2)v. \quad (14c)$$

Due to the regularity of the equations, we can include the boundaries, which lead to a compact state space that is a rectangular box. It is easy to visualize w_φ and Ω_φ since w_φ is constant on the vertical planes $u = \text{const.}$ while Ω_φ is constant on the horizontal planes $v = \text{const.}$ The boundaries are thereby given by a base $v = 0$ and top $v = 1/\sqrt{3}$, representing $\Omega_\varphi = 0, 1$, respectively; the sides $u = \pm\sqrt{2}$ correspond to $w_\varphi = 1$ (since $\Omega_V = \frac{V}{3H^2} = \frac{3}{2}(2 - u^2)v^2$, it follows that $\Omega_V = 0$ on these boundaries); the sides $\bar{\varphi} = \pm\pi$ yield equations that are identical to those obtained from a constant potential $V = \Lambda > 0$. Apart from the boundary $v = 1/\sqrt{3}$ ($\Omega_\varphi = 1$), the equations on the boundaries are all easily solved, see [4]. Note further that the state space can be viewed as being divided into a central slab $-1 < u < 1$, in which $w_\varphi < 0$ where thereby v and Ω_φ are increasing, and two outer slabs $1 < u^2 < 2$ in which w_φ satisfies $0 < w_\varphi < 1$ and where v and Ω_φ are decreasing, as follows from (14c).

2.2 Dynamical systems analysis

Due to the symmetry $\varphi \mapsto -\varphi$ of the potential the dynamical system (14) admits the discrete symmetry

$$(\bar{\varphi}, u) \mapsto -(\bar{\varphi}, u), \quad (15)$$

which leads to that orbits (i.e., solution trajectories) occur in pairs related by this symmetry. The global dynamics of the present models is further restricted by the monotonic function:

$$3H^2 = \frac{V(\bar{\varphi})}{\Omega_V} = \frac{2V(\bar{\varphi})}{3(2-u^2)v^2}, \quad (16a)$$

$$(3H^2)' = -2(1+q)(3H^2) = -3(1-3v^2+3(uv)^2)(3H^2), \quad (16b)$$

where

$$q = -\frac{a\ddot{a}}{\dot{a}^2} = -(1+H'/H) = \frac{1}{2}[1+9(u^2-1)v^2] \quad (17)$$

is the deceleration parameter; since $3H^2 = 2V(\bar{\varphi})/3(2-u^2)v^2$ is strictly monotonically decreasing in the interior state space $(\bar{\varphi}, u, v)$ due to that $1+q$ and $1-3v^2+3(uv)^2$ then are positive, it follows that there are no interior fixed points or recurring orbits in the interior state space — all interior orbits begin and end on the boundaries. Note further that an orbit is accelerating ($q < 0$) when it is inside a trough given by the parabola-like profile $9(1-u^2)v^2 = 1$, see [4] for figures and further details.

The form of the orbits on the invariant boundaries $v = 0$ and $u = \pm\sqrt{2}$ is independent of the potential. First, the base of the state space, $v = 0$, forms the Friedmann-Lemaître (FL) invariant boundary set with $\Omega_\varphi = 0$, $\Omega_m = 1$. Since $\bar{\varphi}' = 0$ and $u' = -\frac{3}{2}(2-u^2)u$ on this set it follows that there are three lines of fixed points:

$$\text{FL}_0^{\varphi*}: \quad (\bar{\varphi}, u, v) = (\bar{\varphi}_*, 0, 0), \quad (18a)$$

$$\text{FL}_\pm^{\varphi*}: \quad (\bar{\varphi}, u, v) = (\bar{\varphi}_*, \pm\sqrt{2}, 0), \quad (18b)$$

with the constant $\bar{\varphi}_*$ satisfying $-\pi \leq \bar{\varphi}_* \leq \pi$, where $w_\varphi = -1$ for $\text{FL}_0^{\varphi*}$ and $w_\varphi = 1$ for $\text{FL}_\pm^{\varphi*}$. These lines of fixed points are connected by heteroclinic orbits³ $\text{FL}_\pm^{\varphi*} \rightarrow \text{FL}_0^{\varphi*}$ that are straight lines with $\bar{\varphi} = \bar{\varphi}_* = \text{constant}$, and thus the evolution of the scalar field is ‘frozen’ on $v = 0$.

Second, the orbits on the $u = \pm\sqrt{2}$ boundaries can also be determined explicitly, as shown in [5, 6]. In particular, all the orbits on the $u = \sqrt{2}$ ($u = -\sqrt{2}$) boundary originate from the kinetic scalar field dominated ‘kinaton’ fixed point K_+^- (K_-^+) at $(\bar{\varphi}, u, v) = (-\pi, \sqrt{2}, 1/\sqrt{3})$ ($(\bar{\varphi}, u, v) = (\pi, -\sqrt{2}, 1/\sqrt{3})$) and end at the line $\text{FL}_+^{\varphi*}$ ($\text{FL}_-^{\varphi*}$), where each fixed point attracts a single orbit, constituting its stable manifold (the two kinaton fixed points K_\pm^\pm are saddles). It is also helpful to note that $\bar{\varphi}$ is increasing when $u > 0$ and decreasing when $u < 0$, which, e.g., determines the flow directions along the boundaries $u = \pm\sqrt{2}$.

Third, the equations for u and v on the boundaries $\bar{\varphi} = \pm\pi$ are the same as those for a constant potential and are easily solved. Furthermore, the straight lines $\text{FL}_0^\pm \rightarrow \text{dS}^\pm$, connecting the boundary FL_0^\pm fixed points at $(\bar{\varphi}, u, v) = (\pm\pi, 0, 0)$ with the boundary

³A heteroclinic orbit is an orbit that connects two different fixed points.

de Sitter fixed points dS^\pm at $(\bar{\varphi}, u, v) = (\pm\pi, 0, 1/\sqrt{3})$, describe the Λ CDM model. There is also an interior Λ CDM orbit $FL_0^0 \rightarrow dS^0$ given by $\bar{\varphi} = 0, u = 0$, connecting a fixed point on the line $FL_0^{\varphi*}$ at $(\bar{\varphi}, u, v) = (0, 0, 0)$ with the de Sitter fixed point dS^0 at $(\bar{\varphi}, u, v) = (0, 0, 1/\sqrt{3})$. Recall that for the Λ CDM solution (where now Ω_φ replaces Ω_Λ)

$$\Omega_\varphi = \frac{\Omega_{\varphi 0}}{\Omega_{m0}e^{-3N} + \Omega_{\varphi 0}}, \quad \Omega_{m0} + \Omega_{\varphi 0} = 1, \quad (19)$$

which yields v since $v = \sqrt{\Omega_\varphi/3}$.

The de Sitter fixed point dS^0 is a hyperbolic sink where all interior orbits end, including those on the scalar field boundary $v = 1/\sqrt{3}$ ($\Omega_m = 0, \Omega_\varphi = 1$). Thus, dS^0 is the future attractor of the present models; see [7] for a rigorous definition of the concept attractor. The orbits $dS^\pm \rightarrow dS^0$ on the $v = 1/\sqrt{3}$ ($\Omega_\varphi = 1$) boundary are the two (due to the discrete symmetry) equivalent *inflationary attractor solutions*, see Figure 2. These orbits are the unstable *center manifold* of the fixed points dS^\pm , while these fixed points are sinks *on* the $\bar{\varphi} = \pm\pi$ boundaries. This latter feature pushes nearby orbits toward the inflationary attractor solutions where the zero eigenvalue strengthens its attracting nature and also enables solutions to stay in a long inflationary quasi-de Sitter epoch in the vicinity of dS^\pm ; cf. the discussion and figures in [2].

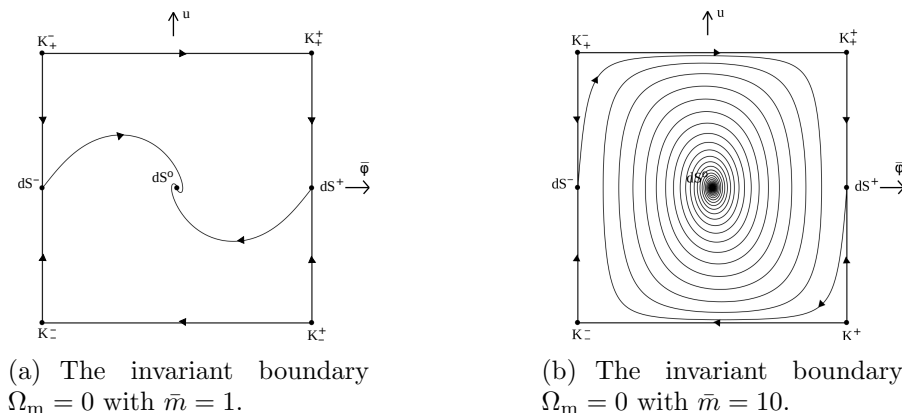


Figure 2: Inflationary attractor (separatrix) orbits $dS^\pm \rightarrow dS^0$ on the $v = 1/\sqrt{3}$ ($\Omega_\varphi = 1$) boundary for $V(\varphi) = \Lambda(1 + \frac{1}{2}\bar{m}^2\varphi^2)$, where $\bar{m} = \frac{m}{\sqrt{2\Lambda}}$.

Of particular interest are the *thawing quintessence attractor solutions*. These are given by the one-parameter set of orbits that originates from $FL_0^{\varphi*}$, one from each fixed point. These orbits form a two-dimensional surface of thawing quintessence ‘attractor’ orbits, illustrated in Figure 3. An observationally required long matter-dominated epoch requires an open set of solutions to be extremely close to the $v = 0$ boundary where orbits are described by frozen values of $\bar{\varphi} = \bar{\varphi}_*$ ending at $FL_0^{\varphi*}$, forming its stable manifold. Nearby orbits shadow these $v = 0$ boundary orbits and are thereby pushed toward the two-dimensional surface of thawing quintessence attractor orbits, i.e. the unstable manifold of $FL_0^{\varphi*}$, which they subsequently shadow. The thawing quintessence attractor orbits thereby describe the thawing quintessence epoch for this open set of shadowing orbits. Finally, note that the inflationary attractor orbits, $dS^\pm \rightarrow dS^0$, form the upper $v = 1/\sqrt{3}$ boundary of the surface of thawing quintessence attractor orbits, see Figure 3.

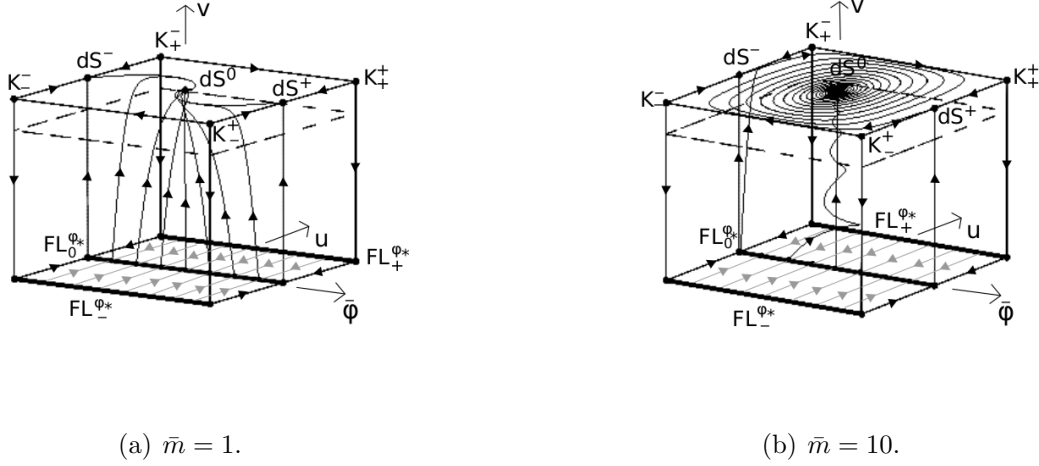


Figure 3: State space $(\bar{\varphi}, u, v)$ depiction of thawing quintessence orbits for the potential $V(\varphi) = \Lambda(1 + \bar{m}^2\varphi^2)$, where $\bar{m} = \frac{m}{\sqrt{2\Lambda}}$, and orbits with frozen $\varphi = \varphi_*$ on the $v = 0$ boundary, responsible for the thawing quintessence mechanism in this state space representation.

3 Models with $V = \Lambda - \frac{1}{2}m^2\varphi^2$

Notably some of the physical properties of some of the solutions of the hilltop potential $V = \Lambda - \frac{1}{2}m^2\varphi^2$ were discussed in [2] and [8], but here we will give a global dynamical systems account of the solution space of these models.

3.1 Dynamical system derivation

To deal with these models we first note that (2a) for the present potential can be written as

$$3H^2 + \frac{1}{2}m^2\varphi^2 = \frac{1}{2}\dot{\varphi}^2 + \Lambda + \rho_m. \quad (20)$$

Next we follow the idea introduced in [9] by defining the following ‘dominant’ quantity

$$D = \sqrt{3H^2 + \frac{1}{2}m^2\varphi^2} = \sqrt{\frac{1}{2}\dot{\varphi}^2 + \Lambda + \rho_m}, \quad (21)$$

which we use to define the following dimensionless bounded variables:

$$\bar{s} = \frac{\sqrt{\Lambda}}{D}, \quad \bar{H} = \frac{\sqrt{3}H}{D}, \quad \bar{\varphi} = \frac{m\varphi}{\sqrt{2}D}, \quad \bar{\Sigma}_\varphi = \frac{\dot{\varphi}}{\sqrt{2}D}, \quad \bar{\Omega}_m = \frac{\rho_m}{D^2}, \quad (22)$$

where $\bar{s} > 0$, $\bar{\Omega}_m > 0$.

It follows from the definitions in (22) and the constraint (2a) that the 5D state vector $(\bar{s}, \bar{H}, \bar{\varphi}, \bar{\Sigma}_\varphi, \bar{\Omega}_m)$ satisfies the two constraints

$$1 = \bar{H}^2 + \bar{\varphi}^2, \quad (23a)$$

$$1 = \bar{\Sigma}_\varphi^2 + \bar{s}^2 + \bar{\Omega}_m, \quad (23b)$$

while $(\bar{s}, \bar{H}, \bar{\varphi}, \bar{\Sigma}_\varphi, \bar{\Omega}_m)$ yield the following evolutions equations, as follows from the definitions (22) and the equations in (2),

$$\frac{d\bar{s}}{d\bar{\tau}} = Q\bar{s}, \quad (24a)$$

$$\frac{d\bar{H}}{d\bar{\tau}} = Q\bar{H} - (2\bar{\Sigma}_\varphi^2 + \bar{\Omega}_m), \quad (24b)$$

$$\frac{d\bar{\varphi}}{d\bar{\tau}} = Q\bar{\varphi} + \tilde{m}\bar{s}\bar{\Sigma}_\varphi, \quad (24c)$$

$$\frac{d\bar{\Sigma}_\varphi}{d\bar{\tau}} = (Q - 2\bar{H})\bar{\Sigma}_\varphi + \tilde{m}\bar{s}\bar{\varphi}, \quad (24d)$$

$$\frac{d\bar{\Omega}_m}{d\bar{\tau}} = 2(Q - \bar{H})\bar{\Omega}_m. \quad (24e)$$

Here we have defined

$$Q = (2\bar{\Sigma}_\varphi^2 + \bar{\Omega}_m)\bar{H} - \tilde{m}\bar{s}\bar{\varphi}\bar{\Sigma}_\varphi, \quad (25)$$

$$\tilde{m} = \frac{2m}{\sqrt{3\Lambda}} = 2\sqrt{\frac{2}{3}}\bar{m}, \quad (26)$$

and introduced a new dimensionless time variable $\bar{\tau}$ defined by

$$\frac{d\bar{\tau}}{dt} = \frac{\sqrt{3}}{2}D, \quad (27)$$

from which it follows that $\bar{\tau}$ is related to the e -fold time N according to

$$\frac{dN}{d\bar{\tau}} = \frac{2}{3}\bar{H}. \quad (28)$$

The constrained dynamical system (23), (24) admits the following discrete symmetries

$$(\bar{\varphi}, \bar{\Sigma}_\varphi) \mapsto -(\bar{\varphi}, \bar{\Sigma}_\varphi), \quad (29a)$$

$$(\bar{\tau}, \bar{H}, \bar{\varphi}) \mapsto -(\bar{\tau}, \bar{H}, \bar{\varphi}), \quad (29b)$$

where combining these two discrete symmetries yield the discrete symmetry $(\bar{\tau}, \bar{H}, \bar{\Sigma}_\varphi) \mapsto -(\bar{\tau}, \bar{H}, \bar{\Sigma}_\varphi)$, which illustrates that the present state space admits time inversion symmetry (this is also the case for positive scalar field potentials, but there we pick out the expanding component; this, however, is not possible for potentials that can change sign since they only yield a single connected state space), whereas (29a) is a consequence of the discrete symmetry $\bar{\varphi} \mapsto -\bar{\varphi}$ of the potential.

It is of interest to consider the following quantities in the new dimensionless bounded variables:

$$\varphi = 2\sqrt{\frac{2}{3}}\tilde{m}^{-1}\left(\frac{\bar{\varphi}}{\bar{s}}\right), \quad V = \Lambda \left[1 - \left(\frac{\bar{\varphi}}{\bar{s}}\right)^2\right], \quad (30a)$$

$$H = \sqrt{\frac{\Lambda}{3}}\left(\frac{\bar{H}}{\bar{s}}\right), \quad \Omega_m = \frac{\bar{\Omega}_m}{\bar{H}^2}, \quad (30b)$$

$$w_\varphi = \frac{\bar{\Sigma}_\varphi^2 + (\bar{\varphi}^2 - \bar{s}^2)}{\bar{\Sigma}_\varphi^2 - (\bar{\varphi}^2 - \bar{s}^2)}, \quad q = -1 + \frac{3}{2}\left(\frac{2\bar{\Sigma}_\varphi^2 + \bar{\Omega}_m}{\bar{\varphi}^2}\right). \quad (30c)$$

Next we solve the constraint (23a) as follows:

$$\bar{H} = \cos \theta, \quad \bar{\varphi} = \sin \theta, \quad (31)$$

while the constraint (23b) is used to globally solve for $\bar{\Omega}_m$, i.e.,

$$\bar{\Omega}_m = 1 - \bar{\Sigma}_\varphi^2 - \bar{s}^2, \quad (32)$$

which leads to the following unconstrained three-dimensional regular dynamical system

$$\frac{d\bar{s}}{d\bar{\tau}} = Q\bar{s}, \quad (33a)$$

$$\frac{d\bar{\Sigma}_\varphi}{d\bar{\tau}} = (Q - 2\cos\theta)\bar{\Sigma}_\varphi + \tilde{m}\bar{s}\sin\theta, \quad (33b)$$

$$\frac{d\theta}{d\bar{\tau}} = (1 + \bar{\Sigma}_\varphi^2 - \bar{s}^2)\sin\theta + \tilde{m}\bar{s}\bar{\Sigma}_\varphi\cos\theta, \quad (33c)$$

where

$$Q = (1 + \bar{\Sigma}_\varphi^2 - \bar{s}^2)\cos\theta - \tilde{m}\bar{s}\bar{\Sigma}_\varphi\sin\theta. \quad (34)$$

It is also of interest to consider the now auxiliary equation

$$\frac{d\bar{\Omega}_m}{d\bar{\tau}} = 2(Q - \cos\theta)\bar{\Omega}_m, \quad (35)$$

which shows that $\bar{\Omega}_m = 1 - \bar{\Sigma}_\varphi^2 - \bar{s}^2 = 0$ is an invariant boundary subset, as is $\bar{s} = 0$. Together these boundary subsets form the boundary of the state space for the state vector $(\bar{s}, \bar{\Sigma}_\varphi, \theta)$. Thanks to the regularity of the dynamical system we now include these boundaries yielding a compact state space for $(\bar{s}, \bar{\Sigma}_\varphi, \theta)$. The state space is thereby given by a torus sliced in half, where the bottom of the sliced torus is given by the invariant boundary set $\bar{s} = 0$ whereas its upper boundary is the invariant set $\bar{\Omega}_m = 1 - \bar{\Sigma}_\varphi^2 - \bar{s}^2 = 0$. The discrete symmetries in (29) take the following form in the system (33):

$$(\bar{\Sigma}_\varphi, \theta) \mapsto -(\bar{\Sigma}_\varphi, \theta), \quad (36a)$$

$$(\bar{\tau}, \theta) \mapsto (-\bar{\tau}, \theta - (2n+1)\pi), \quad n \in \mathbb{Z} \quad (36b)$$

where $\theta \mapsto \theta - (2n+1)\pi$ results in $(\cos\theta, \sin\theta) \mapsto -(\cos\theta, \sin\theta)$. Due to the two discrete symmetries, one can always relate one interior state space orbit to three others, except for when $\bar{\Sigma}_\varphi = 0$, which yields the two ‘interior’ Λ CDM orbits with $\bar{\Sigma}_\varphi = 0$, $\sin\theta = 0$ and the two boundary orbits with $\bar{\Sigma}_\varphi = 0$, $\bar{s} = 0$, discussed below.

3.2 Dynamical systems analysis

We first note that

$$M = \sqrt{\frac{3}{\Lambda}} H = \frac{\bar{H}}{\bar{s}} = \frac{\cos\theta}{\bar{s}} \quad (37)$$

is a strictly monotonically decreasing function in the interior state space, i.e, when $\bar{s} > 0$ and $\bar{\Omega}_m > 0$, since (24) leads to

$$\frac{dM}{d\bar{\tau}} = -\frac{2\bar{\Sigma}_\varphi^2 + \bar{\Omega}_m}{\bar{s}} = -\frac{1 + \bar{\Sigma}_\varphi^2 - \bar{s}^2}{\bar{s}} < 0, \quad (38)$$

and hence there are no interior state space fixed points or recurring orbits, which brings the boundary subsets of the state space into focus.

The invariant $\bar{s} = 0$ boundary set

The equations on the $\bar{s} = 0$ boundary are obtained from (33) by setting $\bar{s} = 0$, which results in

$$\frac{d\bar{\Sigma}_\varphi}{d\bar{\tau}} = -(1 - \bar{\Sigma}_\varphi^2)\bar{\Sigma}_\varphi \cos \theta, \quad (39a)$$

$$\frac{d\theta}{d\bar{\tau}} = (1 + \bar{\Sigma}_\varphi^2) \sin \theta, \quad (39b)$$

which thereby yields a system of equations that are independent of \tilde{m} . The state space is a circular strip with $\bar{\Sigma}_\varphi = -1$ as its invariant inner circle boundary and $\bar{\Sigma}_\varphi = +1$ as the invariant outer circle boundary. Due to the discrete symmetries in (36), the state space is divided into four disjoint invariant regions with the invariant boundary subsets and the invariant inner subsets $\bar{\Sigma}_\varphi = 0$; $\theta = 2n\pi$ and $\theta = (2n + 1)\pi$, $n \in \mathbb{Z}$, i.e., $\sin \theta = 0$, $\cos \theta = \pm 1$, as their boundaries.

The intersections of these one-dimensional invariant sets form 6 fixed points. There are four scalar field kinetic energy dominated *kinaton fixed points* given by

$$K_\epsilon^\pm = \{(\bar{s}, \bar{\Sigma}_\varphi, \cos \theta) = (0, \epsilon, \pm 1)\}, \quad (40)$$

where $\epsilon = 1$ or $\epsilon = -1$. The superscript in K_ϵ^\pm denotes if $\cos \theta = \bar{H}$ is equal to 1 or -1 , a nomenclature that we will use throughout, while the value of the subscript ϵ denotes if $\bar{\Sigma}_\varphi = -1$ or if $\bar{\Sigma}_\varphi = +1$. The discrete symmetry (36a) results in that the fixed points with the same superscript have the same eigenvalues irrespective of the sign of ϵ while the discrete symmetry (36b) yields eigenvalues with opposite signs for fixed points with the same value of ϵ but with an opposite sign of \bar{H} . On the boundary $\bar{s} = 0$ the fixed points K_\pm^+ are hyperbolic sources while K_\pm^- are hyperbolic sinks.

In addition to the four kinaton fixed points there are the two *Friedman-Lemaître fixed points* given by

$$FL^\pm = \{(\bar{s}, \bar{\Sigma}_\varphi, \cos \theta) = (0, 0, \pm 1)\}. \quad (41)$$

On the $\bar{s} = 0$ boundary both these fixed points are hyperbolic saddles. Finally, we note that the dynamical system (39) is integrable, admitting the following conserved quantity

$$\bar{\Sigma}_\varphi \sin \theta = k(1 - \bar{\Sigma}_\varphi^2). \quad (42)$$

Note the invariant $\bar{\Sigma}_\varphi = 0$ ($k = 0$) subset for which $\bar{\Omega}_m = 1$ and $w_\varphi = -1$. The orbit structure on $\bar{s} = 0$ is given in Figure 4.

The invariant $\bar{\Omega}_m = 0$ boundary set

The equations on this subset are obtained by setting $\bar{\Omega}_m = 1 - \bar{\Sigma}_\varphi^2 - \bar{s}^2 = 0$ in (33). In this case $M = \bar{H}/\bar{s} = \cos \theta/\bar{s}$ yields

$$\frac{dM}{d\bar{\tau}} = -\frac{2\bar{\Sigma}_\varphi^2}{\bar{s}} = -\frac{2(1 - \bar{s}^2)}{\bar{s}}; \quad \left. \frac{d^2M}{d\bar{\tau}^2} \right|_{\bar{s}=1} = 0, \quad \left. \frac{d^3M}{d\bar{\tau}^3} \right|_{\bar{s}=1} = -4\tilde{m}^2 \sin^2 \theta. \quad (43)$$

Thus, M is monotonically decreasing everywhere on this subset except possibly at $\bar{s} = 1$, $\bar{\Sigma}_\varphi = 0$; but, as follows from the last two of the above equations, M is also

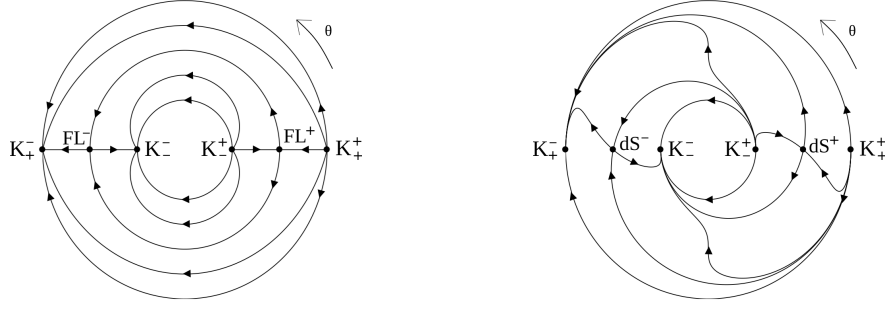


Figure 4: Orbit structure on the $\bar{s} = 0$ (figure to the left) and $\bar{\Omega}_m = 0$ (figure to the right) boundaries, where in the latter case the orbits have been projected onto the plane $\bar{s} = 0$.

monotonically decreasing when $\bar{s} = 1$, $\bar{\Sigma}_\varphi = 0$, *except at the two de Sitter fixed points* with $\sin \theta = 0$,

$$dS^\pm = \{(\bar{s}, \bar{\Sigma}_\varphi, \cos \theta) = (1, 0, \pm 1)\}, \quad (44)$$

where both are hyperbolic saddles on the boundary subset $\bar{\Omega}_m = 0$; for the orbit structure, see Figure 4.

The interior invariant ΛCDM^\pm sets

In addition to the above boundary subsets there are also the interior expanding and contracting ΛCDM^\pm subsets given by two orbits parameterized by \bar{s} according to

$$\Lambda\text{CDM}^+ : \quad \bar{\Sigma}_\varphi = 0, \quad \sin \theta = 0, \quad \cos \theta = 1, \quad \frac{d\bar{s}}{d\bar{\tau}} = (1 - \bar{s}^2)\bar{s}, \quad (45a)$$

$$\Lambda\text{CDM}^- : \quad \bar{\Sigma}_\varphi = 0, \quad \sin \theta = 0, \quad \cos \theta = -1, \quad \frac{d\bar{s}}{d\bar{\tau}} = -(1 - \bar{s}^2)\bar{s}, \quad (45b)$$

respectively, i.e., $\theta = 2n\pi$ ($\theta = (2n + 1)\pi$), $n \in \mathbb{Z}$, for the expanding ΛCDM^+ (contracting ΛCDM^-) subset. Note that $\bar{\Omega}_m = 1 - \bar{s}^2$ and hence that $\frac{d\bar{\Omega}_m}{d\bar{\tau}} = \mp 2(1 - \bar{\Omega}_m)\bar{\Omega}_m$ for these two subsets. Note further that the expanding ΛCDM^+ (contracting ΛCDM^-) subset is given by the heteroclinic orbit $\text{FL}^+ \rightarrow \text{dS}^+$ ($\text{dS}^- \rightarrow \text{FL}^-$).

It follows from the monotonic function M and the structure on the invariant boundary sets that all interior orbits are heteroclinic orbits. We therefore now complete the dynamical systems analysis by situating the stability analysis of the fixed points in the full three-dimensional state space $(\bar{s}, \bar{\Sigma}_\varphi, \theta)$. Note, however, that this analysis follows from combining the results of the above subsets, in particular, use Figure 4 in combination with the ΛCDM^\pm heteroclinic orbits $\text{FL}^+ \rightarrow \text{dS}^+$ and $\text{dS}^- \rightarrow \text{FL}^-$ to obtain an intuitive picture.

Fixed points and their stability

All fixed points satisfy $\bar{\varphi} = \sin \theta = 0$ and $\bar{H} = \cos \theta = \pm 1$ and due to the discrete symmetry (36b) it follows that they always appear in pairs, one corresponding to expansion and one to contraction, where the absolute values of the eigenvalues are the same but where $\bar{\tau} \mapsto -\bar{\tau}$ in (36b) leads to that they have opposite signs.

$\boxed{K_\epsilon^\pm}$ Due to the discrete symmetries (36) it suffices to calculate the eigenvalues of one of the four *kinaton fixed points* since the eigenvalues for the other ones then follow trivially. The kinaton fixed points K_\pm^+ are hyperbolic sources while K_\pm^- are hyperbolic sinks.

$\boxed{dS^\pm}$ The *de Sitter fixed point* dS^+ is a hyperbolic saddle with an eigenvalue -2 with an eigenvector along the expanding ΛCDM^+ orbit and two eigenvalues $\pm\sqrt{1+\tilde{m}^2}-1$ with eigenvectors on the scalar field boundary $\bar{\Omega}_m = 0$, forming a saddle on this boundary, see Figure 4. Thus, there is a one-parameter set of orbits ending at dS^+ .⁴ As follows from (36b), the eigenvalues of dS^- have the opposite signs and is thereby also a hyperbolic saddle; thus there is just one negative eigenvalue with an eigenvector on the $\bar{\Omega}_m = 0$ boundary, whereas a one-parameter set of orbits originates from dS^- .

$\boxed{FL^\pm}$ Among all the fixed points, the *Friedmann-Lemaître fixed point* FL^+ is the most interesting one from a quintessence perspective since it is from this fixed point the one-parameter set of quintessence attractor orbits originate from. Note further that the attractor mechanism of these orbits is given by the stable manifold of FL^+ , given by the orbits $K_\pm^+ \rightarrow FL^+$ with $\bar{s} = 0$, $\theta = 2n\pi$, $n \in \mathbb{Z}$, (see Figure 4), which pushes an open set of nearby orbits toward the unstable manifold of quintessence attractor orbits, which they thereafter shadow and thereby are approximated by. Note further that a long matter-dominated epoch requires solutions to be very close to the FL^+ fixed point.

Finally, note that there is a one-parameter set of orbits ending at the fixed point FL^- (its stable manifold), including the ΛCDM^- orbit, although nearby orbits are pushed away from this subset of orbits by the unstable manifold, given by the orbits $FL^- \rightarrow K_\pm^-$ with $\bar{s} = 0$, $\theta = (2n+1)\pi$, $n \in \mathbb{Z}$, toward the sinks K_\pm^- .

Let us now take a closer look at the quintessence attractor subset of orbits and let us without loss of generality set $\theta = 0$. Then a linear analysis of FL^+ yield the following linear solution

$$\bar{s} = \bar{s}_1 e^{\bar{\tau}}, \quad \bar{\Sigma}_\varphi = \sigma_1 e^{-\bar{\tau}}, \quad \theta = \theta_1 e^{\bar{\tau}}. \quad (46)$$

The quintessence attractor orbits are given by the unstable manifold of FL^+ , i.e. by setting $\sigma_1 = 0$. Recall that matter-dominance requires orbits to be close to FL^+ , where they are pushed toward the unstable manifold of quintessence attractor orbits by the stable manifold associated with the eigenvalue -1 , corresponding to the orbits $K_\pm^+ \rightarrow FL^+$ with $\bar{s} = 0$ and $\theta = 0$.

It is of interest to obtain a better approximation for the unstable manifold than the linear approximation in (46) by series expanding in $\exp(\bar{\tau})$. However, since the variables in the constrained dynamical system (23), (24) are more closely connected to the physical quantities we are interested in and since it is more natural to use

⁴This one-parameter set of orbits, as well as those mentioned below, has two branches related by a discrete symmetry; for brevity, however, we only refer to them as one-parameter sets of orbits.

approximations for \bar{H} and $\bar{\varphi}$ rather than θ we make a series expansion in $\exp(\bar{\tau})$ for this system; when truncated at $\exp(3\bar{\tau})$ this yields

$$\bar{s} \approx \bar{s}_1 e^{\bar{\tau}} \left[1 - \frac{1}{4}(2\bar{s}_1^2 + \bar{\varphi}_1^2) e^{2\bar{\tau}} \right], \quad (47a)$$

$$\bar{H} \approx 1 - \frac{1}{2}\bar{\varphi}_1^2 e^{2\bar{\tau}}, \quad (47b)$$

$$\bar{\varphi} \approx \bar{\varphi}_1 e^{\bar{\tau}} \left[1 - \left(\frac{\bar{\varphi}_1^2}{4} + \frac{\bar{s}_1^2}{6}(3 - \tilde{m}^2) \right) e^{2\bar{\tau}} \right], \quad (47c)$$

$$\bar{\Sigma}_\varphi \approx \frac{1}{3}\tilde{m}\bar{s}_1\bar{\varphi}_1 e^{2\bar{\tau}}, \quad (47d)$$

$$\bar{\Omega}_m \approx 1 - \bar{s}_1^2 e^{2\bar{\tau}}, \quad (47e)$$

which leads to

$$\varphi \approx \varphi_* \left(1 + \frac{1}{6}\tilde{m}^2\bar{s}_1^2 e^{2\bar{\tau}} \right), \quad (48a)$$

$$w_\varphi \approx -1 + \frac{2\tilde{m}^2\bar{s}_1^2\bar{\varphi}_1^2}{9(\bar{s}_1^2 - \bar{\varphi}_1^2)} e^{2\bar{\tau}}, \quad (48b)$$

$$\Omega_m \approx 1 - (\bar{s}_1^2 - \bar{\varphi}_1^2) e^{2\bar{\tau}}, \quad (48c)$$

$$V \approx \Lambda \left[1 - \left(\frac{\bar{\varphi}_1}{\bar{s}_1} \right)^2 \left(1 + \frac{1}{3}\tilde{m}^2\bar{s}_1^2 e^{2\bar{\tau}} \right) \right], \quad (48d)$$

where $\varphi_* \equiv 2\sqrt{\frac{2}{3}}\bar{\varphi}_1/(\tilde{m}\bar{s}_1)$ and hence $\Lambda(\bar{\varphi}_1/\bar{s}_1)^2 = \frac{1}{2}m^2\varphi_*^2$.

The potential is thereby past asymptotically positive when $\bar{s}_1^2 > \bar{\varphi}_1^2$, see Figure 5 for the depiction of $V(\varphi) = 0$ in the state space. Moreover, Ω_φ and $1 + w_\varphi$ are positive since $\Omega_\varphi \approx (\bar{s}_1^2 - \bar{\varphi}_1^2) e^{2\bar{\tau}}$ and $1 + w_\varphi \approx \frac{2\tilde{m}^2\bar{s}_1^2\bar{\varphi}_1^2}{9(\bar{s}_1^2 - \bar{\varphi}_1^2)} e^{2\bar{\tau}}$. The condition $\bar{s}_1^2 > \bar{\varphi}_1^2$ thereby leads to a one-parameter set of *thawing quintessence attractor solutions* with w_φ initially increasing from the past asymptotic value $w_\varphi = -1$ and where Ω_m is initially decreasing from its past asymptotic matter-dominated value $\Omega_m = 1$, where $\bar{\varphi}_1 = 0$ ($\varphi_* = 0$) corresponds to the expanding ΛCDM^+ orbit. However, the potential is past asymptotically negative when $\bar{s}_1^2 < \bar{\varphi}_1^2$, which leads to that Ω_φ and $1 + w_\varphi$ decrease to negative values from their past asymptotic zero values, i.e., this leads to a one-parameter set of *freezing quintessence attractor solutions* early during their evolution.

Note, however, the following: Apart from the ΛCDM^+ orbit and the one-parameter set of orbits ending with a big crunch at FL^- , which includes the ΛCDM^- orbit, all orbits, including the freezing quintessence attractor solutions, end at one of the fixed points K_\pm^\mp where $w_\varphi = 1$. Furthermore, it follows from the monotonic function M and the local fixed point analysis and the orbit structure on the $\bar{s} = 0$ and $\bar{\Omega}_m = 0$ boundaries that all initially expanding solutions ($H > 0$) originate from K_\pm^+ (the generic case), FL^+ (the one-parameter set of quintessence attractor solutions) and dS^+ (the orbits $\text{dS}^+ \rightarrow \text{K}_\pm^-$ on the $\bar{\Omega}_m = 0$ boundary, see Figure 4). These orbits end at K_\pm^- (the generic case) and at FL^- (a one-parameter set, including the $\text{FL}^+ \rightarrow \text{FL}^-$ orbits on the $\bar{s} = \bar{\Sigma}_\varphi = 0$ subset, see Figure 4) and at dS^- (the orbits $\text{K}_\pm^+ \rightarrow \text{dS}^-$ on the $\bar{\Omega}_m = 0$ boundary, see Figure 4).

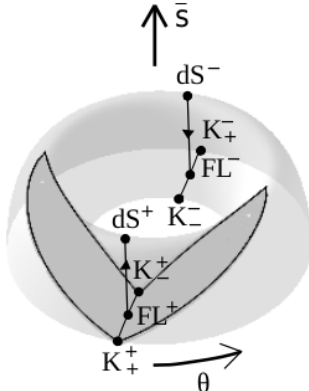


Figure 5: The $V(\varphi) = 0$ surface ‘originating’ from $\theta = 0$; in addition, there is a corresponding $V(\varphi) = 0$ surface, not depicted in order to avoid clutter, at $\theta = \pi$, since $V = 0 \Rightarrow \bar{s} = |\bar{\varphi}| = |\sin \theta|$.

Thus all interior orbits ($\bar{s} > 0$, $\bar{\Omega}_m > 0$), apart from the ΛCDM^+ orbit, reach a point of maximum expansion (where $H = 0$ and thus $\bar{H} = \cos \theta = 0$, i.e., $\theta = \pi/2 + n\pi$, $n \in \mathbb{Z}$) and then contract to a big crunch singularity. As will be shown below, observationally viable thawing quintessence models more or less shadow one of the following two discrete symmetry related heteroclinic orbit sequences $\text{FL}^+ \rightarrow \text{dS}^+ \rightarrow \text{K}_+^-$, $\text{FL}^+ \rightarrow \text{dS}^+ \rightarrow \text{K}_-^-$; they thereby end at a contracting kinaton state with $\bar{H} = -1$ ($H \rightarrow -\infty$) and $w_\varphi = 1$. Examples of orbits are given in Figure 6. Compare these detailed results with those in [2].

3.3 The quintessence attractor subset

As shown above, the quintessence attractor subset is the one-parameter set of orbits forming the unstable manifold of FL^+ . This subset is in turn divided into two parts: the thawing and freezing orbits, where only the thawing quintessence attractor subset contains solutions of observational interest, namely those that have sufficiently large Ω_φ and accelerated expansion during the last few billion years up to the present time (see the discussion in [8]). Since these solutions satisfy $V(\varphi) > 0$, $\rho_\varphi \geq 0$, $\Omega_\varphi \geq 0$, from their asymptotic past to the present time, and since thereby $v = \sqrt{\Omega_\varphi/3}$ is well defined for this time period we can use the previous formulation for bounded $\lambda(\varphi)$ for their evolution to the present time. Figure 7 depicts three thawing attractor solutions in the two state spaces $(\bar{\varphi}, u, v)$ and $(\bar{s}, \bar{\Sigma}_\varphi, \theta)$ from their asymptotic past at FL^+ to the present time (characterized by $\Omega_\varphi = 0.68$ and denoted by a ring in Figure 7) and beyond, where only the $(\bar{s}, \bar{\Sigma}_\varphi, \theta)$ state space yields their entire evolution and their final contraction to a big crunch at the kinaton fixed point K_+^- .

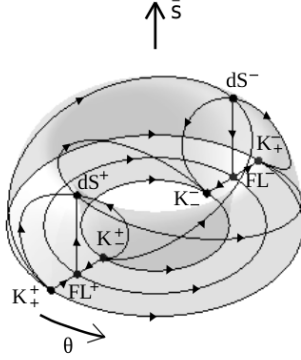


Figure 6: Examples of orbits. The expanding and contracting Λ CDM $^\pm$ orbits are given by $FL^+ \rightarrow dS^+$ and $dS^- \rightarrow FL^-$, respectively. Viable thawing quintessence models more or less shadow one of the following two discrete symmetry related heteroclinic orbit sequences $FL^+ \rightarrow dS^+ \rightarrow K_-^-$, $FL^+ \rightarrow dS^+ \rightarrow K_+^-$; they thereby end at a contracting kinaton state with $\bar{H} = -1$ ($H \rightarrow -\infty$) and $w_\varphi = 1$.

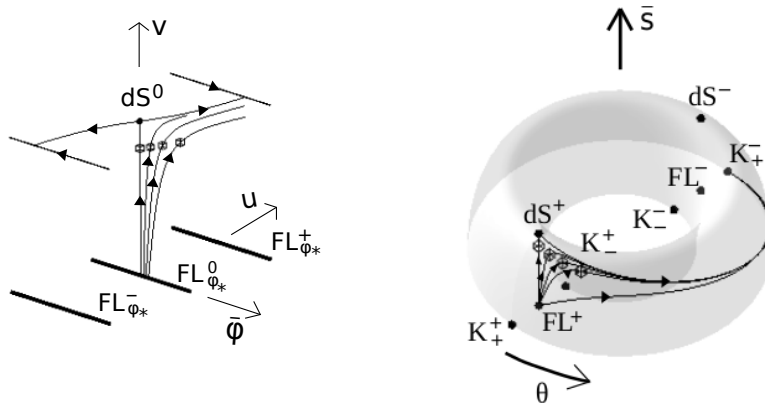


Figure 7: Thawing quintessence attractor solutions (and the Λ CDM $^\pm$ solution) in the $(\bar{\varphi}, u, v)$ state space and the corresponding ones in the $(\bar{s}, \bar{\Sigma}_\varphi, \theta)$ state space. The ring denotes when $\Omega_\varphi = 0.68$.

Acknowledgments

A. A. is supported by FCT/Portugal through FCT/Tenure 2023.15700.TENURE.003/CP00055/CT00003, CAMGSD, IST-ID, grant No. UID/4459/2025, and projects 2024.04456.CERN, and H2020-MSCA-2022-SE Ein-

steinWaves, GA No. 101131233. A.A. would also like to thank the CMA-UBI in Covilhã for kind hospitality. C. U. would like to thank the CAMGSD, Instituto Superior Técnico in Lisbon for kind hospitality.

References

- [1] DESI Collaboration and M. Abdul-Karim et al. Desi dr2 results. ii. measurements of baryon acoustic oscillations and cosmological constraints. *Phys. Rev. D*, 112:083515, Oct 2025.
- [2] Gary Felder, Andrei Frolov, Lev Kofman, and Andrei Linde. Cosmology with negative potentials. *Phys. Rev. D*, 66:023507, Jul 2002.
- [3] William J. Wolf, Carlos García-García, and Pedro G. Ferreira. Robustness of dark energy phenomenology across different parameterizations. *Journal of Cosmology and Astroparticle Physics*, 2025(05):034, may 2025.
- [4] A. Alho, C. Uggla, and J. Wainwright. Quintessence from a state space perspective. *Physics of the Dark Universe*, **39**:101146, 2023.
- [5] A. Alho and C. Uggla. Quintessential α -attractor inflation: A dynamical systems analysis. *Journal of Cosmology and Astroparticle Physics*, **11**:083, 2023.
- [6] A. Alho, W. C. Lim, and C. Uggla. Cosmological global dynamical systems analysis. *Class. Quantum Grav.*, **39**:145010, 2022.
- [7] J. Wainwright and G. F. R. Ellis. *Dynamical systems in cosmology*. Cambridge University Press, 1997.
- [8] Ujjaini Alam, Varun Sahni, and Alexei A Starobinsky. Can dark energy be decaying? *Journal of Cosmology and Astroparticle Physics*, 2003(04):002, apr 2003.
- [9] C. Uggla and H. Zur-Muhlen. Compactified and reduced dynamics for locally rotationally symmetric bianchi type ix perfect fluid models. *Classical and Quantum Gravity*, 7(8):1365, aug 1990.